

SWIFT OBSERVATIONS OF SMC X-3 DURING ITS 2016-2017 SUPER-EDDINGTON OUTBURST

SHAN-SHAN WENG¹, MING-YU GE², HAI-HUI ZHAO¹, WEI WANG^{3,4}, SHUANG-NAN ZHANG^{2,4,5}, WEI-HAO BIAN¹, QI-RONG YUAN¹

¹ Department of Physics and Institute of Theoretical Physics, Nanjing Normal University, Nanjing 210023, China

² Key Laboratory of Particle Astrophysics, Institute of High Energy Physics, Chinese Academy of Sciences, Beijing 100049, China

³ School of Physics and Technology, Wuhan University, 430072 Wuhan, Hubei, China

⁴ National Astronomical Observatories, Chinese Academy of Sciences, Beijing 100012, China and

⁵ University of the Chinese Academy of Sciences, Beijing, China

Draft version July 8, 2021

ABSTRACT

The Be X-ray pulsar, SMC X-3 underwent a giant outburst from 2016 August to 2017 March, which was monitored with the *Swift* satellite. During the outburst, its broadband flux increased dramatically, and the unabsorbed X-ray luminosity reached an extreme value of $\sim 10^{39}$ erg/s around August 24. Using the *Swift*/XRT data, we measure the observed pulse frequency of the neutron star to compute the orbital parameters of the binary system. After applying the orbital corrections to *Swift* observations, we find that the spin frequency increases steadily from 128.02 mHz on August 10 and approach to spin equilibrium ~ 128.74 mHz in 2017 January with an unabsorbed luminosity of $L_X \sim 2 \times 10^{37}$ erg/s, indicating a strong dipolar magnetic field $B \sim 6.8 \times 10^{12}$ G at the neutron star surface. The spin-up rate is tightly correlated with its X-ray luminosity during the super-Eddington outburst. The pulse profile in the *Swift*/XRT data is variable, showing double peaks at the early stage of outburst and then merging into a single peak at low luminosity. Additionally, we report that a low temperature ($kT \sim 0.2$ keV) thermal component emerges in the phase-averaged spectra as the flux decays, and it may be produced from the outer truncated disk or the boundary layer between the exterior flow and the magnetosphere.

Keywords: accretion, accretion disks — stars: neutron — pulsars: general — X-rays: binaries — X-rays: individual (SMC X-3)

1. INTRODUCTION

High-mass X-ray binaries contribute a large fraction of X-ray emission in normal galaxies, and they are believed to reflect the recent star-formation activities in their host galaxies (e.g. Grimm et al. 2002; Mineo et al. 2012). According to the states of their optical companions, high-mass X-ray binaries can be subdivided into supergiant X-ray binaries and Be/X-ray binaries (BeXBs). A BeXB consists of a Be star and a compact object. Virtually, all confirmed compact objects in BeXBs are neutron stars (NSs), and all these systems show X-ray pulsations (see Reig 2011 for reviews). As young systems, NSs in BeXBs have high magnetic field ($B > 10^{10}$ G); therefore, BeXBs provide unique natural laboratories for studying physics in extremely strong gravity and magnetic fields.

The direct measurement of a NS magnetic field strength can be achieved from the detection of a cyclotron scattering resonance feature (e.g. Coburn et al. 2002; Yan et al. 2012; Fürst et al. 2014; Walter et al. 2015, and references therein). Additionally, investigating the interaction between the magnetosphere and the accretion matter, we can acquire the information of NS magnetic field indirectly (e.g. Weng & Zhang 2011; Shi et al. 2015; Christodoulou et al. 2016). That is, the effect of the magnetic field strength manifest itself by the size of its magnetosphere co-rotating with the central NS. The boundary of the magnetosphere is determined where the ram pressure of in-falling flow is balanced by magnetic pressure; thus, it expands with field strength and

decreases with mass accretion rate (Lamb et al. 1973; Ghosh & Lamb 1979). As the accretion rate decreases below the critical value, the magnetospheric radius (R_m)

grows beyond the corotation radius ($R_{co} = \sqrt[3]{\frac{GMP^2}{4\pi^2}}$), at which the Keplerian angular frequency is equal to the NS spin frequency, and the centrifugal barrier spins away accretion matter. If most of material is prevented from accreting onto NS, X-ray flux and pulsation decay sharply in a few days, i.e. the “propeller” effect (e.g. Cui 1997; Campana et al. 2014). Alternatively, the magnetosphere is penetrated into the corotation radius at high luminosity, leading to the spin-up of a NS. If NSs are close to spin equilibrium, their magnetic fields can be estimated from long-term averaged spin parameters and X-ray luminosity (e.g. Klus et al. 2014; Shi et al. 2015). Meanwhile, the torque reversals between steady spin-up and spin-down are commonly shown in BeXBs (e.g. Bildsten et al. 1997).

Besides the long-term average spin evolution, the instantaneous torque measurements during episodic outbursts are essential to test accretion torque theories. Transient BeXBs experience periodic and less energetic ($L_X < 10^{37}$ erg/s) outbursts or rare giant outbursts, which are referred to as type I and type II outbursts, respectively (Reig 2011). The tight relationships between spin-up rate and (pulsed) flux detected in the luminous outbursts of BeXBs (e.g. A0535+262 and 2S 1417-624) are interpreted as the sign of transient accretion disks around NSs, which are supported by the detection of simultaneous quasi-periodic oscillations (QPOs) (Finger et al. 1996; Sartore et al.

2015). It is worth to note that a small number of sources (e.g. SMC X-1, LMC X-4, 4U 0115+63, V0332+53) can reach a peak X-ray luminosity in excess of 10^{38} erg/s (e.g. Li et al. 2011; Mushtukov et al. 2015b, and references therein). Intriguingly, a growing number of ultraluminous X-ray sources (ULXs) in nearby galaxies have been found to exhibit coherent pulsations (Bachetti et al. 2014; Fürst et al. 2016; Israel et al. 2016, 2017), indicating a connection to X-ray pulsars (Shao & Li 2015; Mushtukov et al. 2015b; Kawashima et al. 2016; King & Lasota et al. 2016; Mushtukov et al. 2017). Nowadays, super-Eddington accretion in magnetized NSs draw more attention (e.g. Ekşi et al. 2015; Pan et al. 2016; Tsygankov et al. 2016; Chen 2017). However, a detailed study on such dramatic phenomena is hampered by the lack of observations.

The Small Magellanic Cloud (SMC) is the second nearest galaxy ($d = 62.1$ kpc; Hilditch et al. 2005; Graczyk et al. 2014; Scowcroft et al. 2016) after the Large Magellanic Cloud, and it has high-mass X-ray binaries in abundance due to the recent star-forming activities (Zaritsky et al. 2002; Sturm et al. 2013; Yang et al. 2017). SMC X-3 (also known as SXP 7.78) was discovered with *SAS 3* X-ray observatory in 1978 (Clark et al. 1978), and was identified as an accreting pulsar with a detected pulsation of 7.78 second (Edge et al. 2004). The spectral type of the optical counterpart is identified as B1–B1.5 with $V = 14.91$ (McBride et al. 2008). The orbital period ~ 44.9 days was detected in both X-ray and optical bands (Corbet et al. 2003; Cowley et al. 2004; Galache et al. 2008; Bird et al. 2012). However, its eccentricity and other orbital parameters are still unknown. Recently, SMC X-3 underwent a giant type II outburst in 2016 with a peak X-ray luminosity of $\sim 10^{39}$ erg/s, and it was monitored in Target of Opportunity mode by *Swift* since 2016 August 10. On 2016 November 8, we reported our preliminary results on analyzing the *Swift* data (Weng et al. 2016), which are the basis of this work. During preparation of this manuscript, Townsend et al. (2017, submitted) investigated the optical and X-ray data (including the *Swift* data) of SMC X-3, and obtained similar orbital parameters of the binary as given in our paper. In this paper, we focus on the *Swift* data and carry out a comprehensive analysis on these data to investigate the physics of super-Eddington accretion around a magnetized NS. The data reduction is described in the next section. In Section 3, we perform the timing analysis and calculate the orbital elements of the binary. In Section 4, we discuss the physical implications of these results and present our main conclusions.

2. DATA REDUCTION

The *MAXI*/GSC was triggered by brightening of SMC X-3 on 2016 August 8 (Negoro et al. 2016), which was confirmed by *Swift* during its survey of the SMC (Kennea et al. 2016). In this paper, we analyze all *Swift* pointing observations taken between 2016 August 10 and 2017 January 1. The *Swift* Gamma Ray Burst Explorer carries three scientific instruments covering a broad energy range of $\sim 0.002 - 150$ keV: the Burst Alert Telescope (BAT), the X-ray Telescope (XRT), and the UV/Optical Telescope (UVOT) (Gehrels et al. 2004). The BAT daily light curve is adopted from Krimm et al.

(2013)¹. Meanwhile, both the XRT and the UVOT data are processed with the packages and tools available in HEASOFT 6.19.

When the source is bright, the observations are carried out in the windowed-timing (WT) mode. While after 2017 January 16, the count rate in 0.5–10 keV is less than 0.5 cts/s, and the observations are performed in the photon-counting (PC) mode without significant pile-up effects (Table 1). For the XRT data, the initial event cleaning is executed with the task `xrtpipeline` using standard quality cuts. The source and background events are extracted from a circle and an annulus region centered at the source position, respectively. The light curves are corrected for the telescope vignetting and point-spread-function losses with the task `xrtlccorr`, and then are subtracted by the scaled background count rate to yield the net light curves (Figure 1). The hardness for each observation is calculated as the ratio of average count rates (CR) in (2.0–10.0 keV)/(0.5–2.0 keV) bands. The source becomes undetected in last three observations, the upper limit of count rates are estimated by using the X-ray image package XIMAGE.

The ancillary response files are created using the task `xrtmkarf` and the latest response files are taken from the CALDB database for the spectral analyses. The spectral fitting is restricted to the 0.6–10 keV energy range due to calibration residuals below 0.6 keV for the WT mode data². For the PC mode data, we employ the C-statistic (Cash 1979) instead of common χ^2 for spectral fitting in 0.3–10 keV because of low count rates and short exposure times. Unfortunately, spectra are unavailable for some observations which have very limited photons (Table 1). The absorption column density along the line of sight to SMC X-3 is difficult to constrain and could yield an extremely small value ($nH < 10^{14}$ cm⁻²) for some of the observations; therefore, we fix it to the Galactic absorption towards the direction of the source (6.57×10^{20} cm⁻², Dickey & Lockman 1990). At the early stage of the outburst, the phase-averaged spectra can be well fitted by an absorbed power-law (PL) model with a photon index of $\sim 0.7 - 1.2$. These results are consistent with those seen in *NuSTAR* data, which can be fitted by a cutoff PL model with a photon index $\sim 0.5 - 0.7$ and a folding energy of $\sim 11 - 15$ keV (Pottschmidt et al. 2016; Tsygankov et al. 2017). During 2016 September 25 and December 12, the soft excess emerges below 1 keV, which can be described by a black-body (BB) emission with $kT \sim 0.1 - 0.2$ keV and $R_{\text{BB}} \sim 10^2 - 10^3$ km. The soft thermal component is variable and contributes a small fraction ($\sim 1 - 3\%$) of total flux in 0.6–10 keV; however, because of the low S/N ratio of band-limited data, we cannot put a tight constraint on this component.

In order to rule out the instrumental influence, we also analyze the XMM-Newton EPIC-pn spectrum observed on 2016 October 14-15 and confirm the existence of the thermal component. The EPIC-MOS data were taken in imaging mode and suffered from the pile-up effect; therefore, we only use the EPIC-pn data which was in timing mode. The data in the first 4.5 kilo seconds are excluded because of background flares, and the

¹ <http://swift.gsfc.nasa.gov/results/transients/>

² see <http://swift.gsfc.nasa.gov/docs/heasarc/caldb/swift/docs/xrt/SWIFTXRT-CALDB-09.pdf>

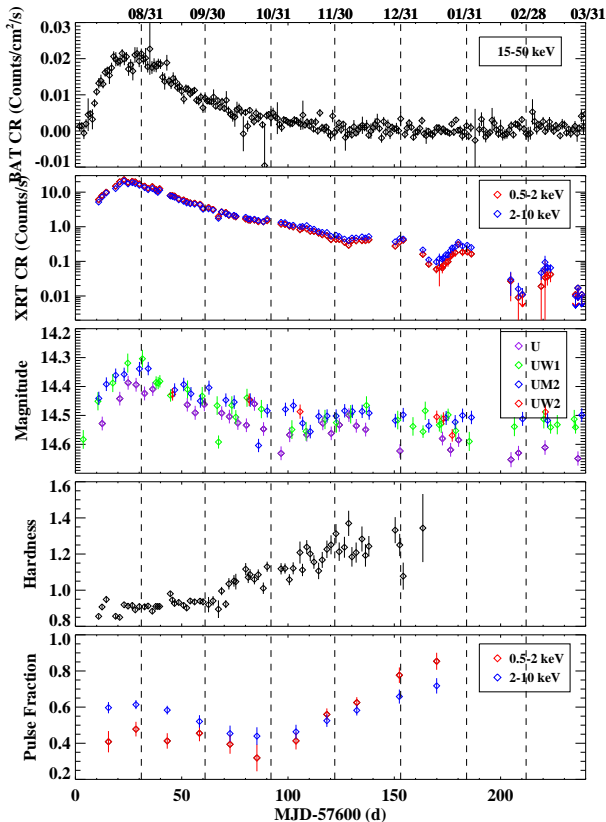


Figure 1. Panels from top to bottom show the light curves from the BAT, XRT, UVOT data, the evolution of the 2–10 keV to 0.5–2 keV hardness ratios, and the pulse fractions, respectively. The hardness ratios after MJD 57765 are not shown in the bottom panel due to large uncertainties.

spectrum is extracted from the rest data with an exposure time of 28 kilo seconds. The EPIC-pn spectrum cannot be well fitted by a single PL model with a reduced χ^2 larger than 2.9. When a cool BB component is added, the reduced χ^2 decreases to 1.07, and it further reduces to 0.75 with including an additional Gaussian line (phabs*(bbodyrad+powerlaw+gauss) in XSPEC, Figure 2). The best fitted parameters are: $nH = 1.4^{+0.2}_{-0.2} \times 10^{21}$ cm $^{-2}$, $kT = 0.19^{+0.01}_{-0.01}$ keV, $Norm_{BB} = 1136^{+560}_{-392}$, $\Gamma = 0.99^{+0.01}_{-0.01}$, $Norm_{PL} = 1.54^{+0.03}_{-0.03} \times 10^{-2}$, $E_1 = 6.65^{+0.10}_{-0.10}$ keV, $\sigma = 0.35^{+0.14}_{-0.10}$ keV, $Norm_{Gau} = 1.64^{+0.53}_{-0.45} \times 10^{-5}$, and $\chi^2/dof = 123.8/165$. More detailed analysis on the XMM-Newton data will be presented elsewhere.

In addition to the pointing data, we include the 27 survey observations (on the SMC) with an average exposure of ~ 60 s for the following photometry. For each observation, we first sum the sky images with `uvotsum`, and then perform aperture photometry with the summed images by using `uvotsource`. A source aperture of radius 5 arcsec and a larger neighbouring source-free region for background are used. The AB magnitudes for all filters are shown in Figure 1.

3. TIMING ANALYSIS & RESULTS

The spin evolution during giant outbursts is crucial for investigating the accretion processes in BeXBs and for determining orbital parameters by using the orbital

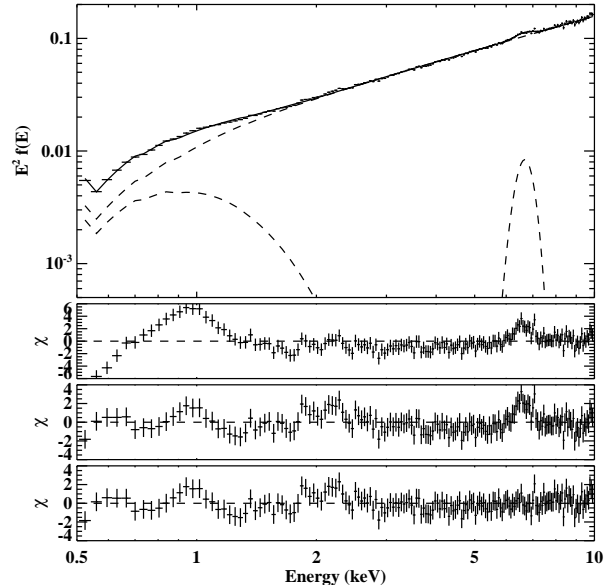


Figure 2. Fitting to the XMM-Newton EPIC-pn spectrum observed on 2016 October 14–15 (ObsID = 0793182901). Panels from top to bottom show the unfolded spectra using the (BB+PL+Gau) model, the fitting residuals for the a single PL model, the (BB+PL) model, and with an additional Gaussian line.

Doppler effect (e.g. Li et al. 2011). Only WT mode data, which have a high time resolution and relatively long exposure time for individual observations (Table 1), are used for the following timing analysis. Before computing the spin frequency, we apply the barycentric correction with the `ftool barycorr` to the source event files (in the range of 0.5–10 keV). The source position is adopted from the 2MASS all sky Catalog of point sources (Cutri et al. 2003). The spin frequency is obtained by folding the observed counts to reach the maximum Pearson χ^2 . The derived values of the observed spin frequency are the same as that presented by the *Fermi*/GBM Pulsar Project³; however, the source becomes faint and below the detection limit of GBM after MJD 57671 (Figure 3).

The background-subtracted light curves with a time bin size of 0.05 s are extracted from the barycentric corrected event files, and are folded over the best frequency. For the purpose of comparing the profiles between observations, the pulse profiles are aligned by the cross correlation function (Figure 4). The energy-dependent pulse profiles make clear that the spectra harden during the peak. The pulse fraction is defined as $PF = (M - N)/(M + N)$, where M and N are the maximum and minimum flux of the profile, respectively. To reduce the statistical error, we calculate the mean pulse fraction in every 15 days, which are shown in the bottom panel of Figure 1.

3.1. Orbital Elements

To study the frequency evolution, the *Doppler* effects of the binary should be considered here. However, the frequency evolution is very fast, so we utilize seven frequency derivatives to describe spin evolution. The detailed processes are described as follows: (1)The spin

³ <http://gammaray.nsstc.nasa.gov/gbm/science/pulsars.html>

Table 1
Log of *Swift*/XRT data

ObsID	Date	Exposure (second)	Mode	R_{Source} (pixel)	$R_{\text{Background}}$ (pixel/pixel)	$L_{0.6-10\text{keV}}$ (10^{37} erg/s)
00034673001	2016-08-10	4671	WT	25	25/50	$35.3^{+0.4}_{-0.4}$
00034673002	2016-08-12	1978	WT	25	25/50	$46.9^{+0.7}_{-0.7}$
00034673003	2016-08-14	935	WT	25	25/50	$59.0^{+1.1}_{-1.1}$
00034673004	2016-08-18	1997	WT	25	25/50	$68.3^{+0.8}_{-0.8}$
00034673005	2016-08-20	2050	WT	25	25/50	$84.0^{+1.0}_{-1.0}$
00034673006	2016-08-22	1958	WT	25	25/50	$90.1^{+0.9}_{-0.9}$
00034673007	2016-08-24	1291	WT	25	25/50	$102.7^{+1.4}_{-1.3}$
00034673008	2016-08-26	504	WT	25	25/50	$98.2^{+1.9}_{-1.9}$
00034673009	2016-08-28	1583	WT	25	25/50	$98.2^{+1.1}_{-1.1}$
00034673010	2016-08-30	953	WT	25	25/50	$88.1^{+1.3}_{-1.3}$
00034673011	2016-09-01	793	WT	25	25/50	$92.9^{+1.6}_{-1.6}$
00034673012	2016-09-03	1932	WT	25	25/50	$78.9^{+1.0}_{-1.0}$
00034673013	2016-09-05	1345	WT	25	25/50	$56.6^{+1.0}_{-1.0}$
00034673014	2016-09-06	2985	WT	25	25/50	$61.1^{+0.6}_{-0.6}$
00034673015	2016-09-07	2977	WT	25	25/50	$61.3^{+0.7}_{-0.7}$
00034673016	2016-09-08	2764	WT	25	25/50	$57.2^{+0.7}_{-0.7}$
00034673017	2016-09-13	2973	WT	25	25/50	$45.1^{+0.5}_{-0.5}$
00034673018	2016-09-14	2979	WT	25	25/50	$44.2^{+0.5}_{-0.5}$
00034673019	2016-09-15	2981	WT	25	25/50	$42.8^{+0.5}_{-0.5}$
00034673020	2016-09-17	3004	WT	25	25/50	$33.5^{+0.4}_{-0.4}$
00034673021	2016-09-19	2918	WT	25	25/50	$30.8^{+0.4}_{-0.4}$
00034673022	2016-09-21	2591	WT	25	25/50	$27.4^{+0.4}_{-0.4}$
00034673023	2016-09-23	2992	WT	25	25/50	$26.0^{+0.4}_{-0.4}$
00034673024	2016-09-25	2610	WT	25	25/50	$24.9^{+0.4}_{-0.4}$
00034673025	2016-09-27	3289	WT	25	25/50	$23.6^{+0.4}_{-0.4}$
00034673026	2016-09-29	2969	WT	25	25/50	$19.3^{+0.4}_{-0.4}$
00034673027	2016-10-01	553	WT	25	25/50	$17.6^{+0.8}_{-0.7}$
00034673028	2016-10-03	1718	WT	25	25/50	$16.2^{+0.4}_{-0.4}$
00034673029	2016-10-06	726	WT	25	25/50	$17.5^{+1.0}_{-0.9}$
00034673030	2016-10-07	2789	WT	25	25/50	$14.9^{+0.3}_{-0.3}$
00034673031	2016-10-09	2839	WT	25	25/50	$13.2^{+0.3}_{-0.3}$
00034673032	2016-10-11	1982	WT	25	25/50	$12.6^{+0.4}_{-0.3}$
00034673033	2016-10-13	2028	WT	25	25/50	$12.2^{+0.3}_{-0.3}$
00034673034	2016-10-14	1199	WT	25	25/50	$11.6^{+0.5}_{-0.4}$
00034673035	2016-10-19	2493	WT	25	25/50	$10.2^{+0.3}_{-0.3}$
00034673036	2016-10-20	2852	WT	25	25/50	$9.62^{+0.26}_{-0.26}$
00034673037	2016-10-21	3435	WT	25	25/50	$9.31^{+0.23}_{-0.22}$
00034673038	2016-10-23	3685	WT	25	25/50	$9.37^{+0.22}_{-0.22}$
00034673039	2016-10-25	3626	WT	25	25/50	$8.51^{+0.21}_{-0.21}$
00034673040	2016-10-27	2959	WT	25	25/50	$7.67^{+0.25}_{-0.25}$
00034673041	2016-10-29	3984	WT	25	25/50	$9.04^{+0.23}_{-0.23}$
00034673042	2016-11-06	5256	WT	25	25/50	$7.16^{+0.18}_{-0.17}$
00034673043	2016-11-04	3973	WT	25	25/50	$7.59^{+0.22}_{-0.22}$
00034673044	2016-11-08	4646	WT	25	25/50	$6.57^{+0.18}_{-0.18}$
00034673045	2016-11-10	4453	WT	25	25/50	$6.30^{+0.18}_{-0.18}$
00088012001	2016-11-13	1803	WT	25	25/50	$5.56^{+0.26}_{-0.26}$
00034673046	2016-11-14	4452	WT	25	25/50	$5.78^{+0.16}_{-0.16}$
00034673047	2016-11-16	4328	WT	25	25/50	$5.91^{+0.19}_{-0.19}$
00034673048	2016-11-18	4628	WT	25	25/50	$5.04^{+0.16}_{-0.15}$
00034673049	2016-11-20	4881	WT	25	25/50	$5.07^{+0.16}_{-0.16}$
00034673050	2016-11-22	3287	WT	25	25/50	$4.21^{+0.17}_{-0.17}$
00034673051	2016-11-24	4484	WT	25	25/50	$3.89^{+0.14}_{-0.14}$
00034673053	2016-11-26	4430	WT	25	25/50	$3.82^{+0.15}_{-0.15}$
00034673054	2016-11-28	4589	WT	25	25/50	$3.37^{+0.14}_{-0.14}$
00034673055	2016-11-30	5026	WT	25	25/50	$3.35^{+0.13}_{-0.12}$
00034673056	2016-12-02	4563	WT	25	25/50	$3.01^{+0.13}_{-0.13}$

Note. — R_{Source} : Radius of source region; $R_{\text{Background}}$: Inner and outer radius of background region;
 $L_{0.6-10\text{keV}}$: Unabsorbed luminosities are calculated with the distance of $d = 62.1$ kpc.

Table 1
Log of *Swift*/XRT data

ObsID	Date	Exposure (second)	Mode	R_{Source} (pixel)	$R_{\text{Background}}$ (pixel/pixel)	$L_{0.6-10\text{keV}}$ (10^{37} erg/s)
00034673057	2016-12-04	4915	WT	25	25/50	$2.57^{+0.12}_{-0.11}$
00034673058	2016-12-06	4917	WT	25	25/50	$2.24^{+0.11}_{-0.11}$
00034673059	2016-12-08	4526	WT	25	25/50	$2.68^{+0.13}_{-0.12}$
00034673060	2016-12-10	4711	WT	25	25/50	$2.70^{+0.11}_{-0.11}$
00034673061	2016-12-12	3073	WT	25	25/50	$2.92^{+0.16}_{-0.16}$
00034673062	2016-12-14	3538	WT	25	25/50	$2.83^{+0.13}_{-0.13}$
00034673063	2016-12-16	4380	WT	25	25/50	$3.08^{+0.13}_{-0.12}$
00034673064	2016-12-28	4189	WT	25	25/50	$2.25^{+0.11}_{-0.11}$
00034673065	2016-12-30	4288	WT	25	25/50	$2.36^{+0.12}_{-0.12}$
00034673066	2017-01-01	2026	WT	25	25/50	$2.30^{+0.19}_{-0.18}$
00034673067	2017-01-10	1179	WT	25	25/50	$1.37^{+0.26}_{-0.23}$
00034673069	2017-01-13	1666	WT	25	25/50	$0.75^{+0.12}_{-0.11}$
00034673071	2017-01-16	768	PC	15	15/30	$0.68^{+0.09}_{-0.08}$
00034673073	2017-01-18	82	PC	15	15/30	... §
00034673074	2017-01-19	445	PC	15	15/30	$0.77^{+0.12}_{-0.11}$
00034673075	2017-01-20	382	PC	15	15/30	$0.83^{+0.12}_{-0.11}$
00034673076	2017-01-21	347	PC	15	15/30	$1.05^{+0.16}_{-0.14}$
00034673077	2017-01-22	329	PC	15	15/30	$1.06^{+0.17}_{-0.15}$
00034673078	2017-01-23	355	PC	15	15/30	$1.38^{+0.17}_{-0.15}$
00034673079	2017-01-24	336	PC	15	15/30	$1.67^{+0.19}_{-0.17}$
00034673080	2017-01-25	235	PC	15	15/30	$1.65^{+0.22}_{-0.19}$
00034673081	2017-01-27	2295	WT	15	15/30	$1.98^{+0.16}_{-0.16}$
00034673082	2017-01-29	237	PC	15	15/30	$1.75^{+0.23}_{-0.20}$
00034673083	2017-01-31	394	PC	15	15/30	$1.86^{+0.17}_{-0.16}$
00034673084	2017-02-02	552	PC	15	15/30	$1.76^{+0.15}_{-0.14}$
00034673087	2017-02-20	138	PC	15	15/30	... §
00034673088	2017-02-24	385	PC	15	15/30	... §
00034673089	2017-02-26	411	PC	15	15/30	... §
00034673091	2017-03-07	198	PC	15	15/30	... §
00034673092	2017-03-08	57	PC	15	15/30	... §
00034673093	2017-03-09	345	PC	15	15/30	$0.46^{+0.13}_{-0.10}$
00034673094	2017-03-10	384	PC	15	15/30	$0.46^{+0.12}_{-0.10}$
00034673095	2017-03-11	350	PC	15	15/30	$0.42^{+0.09}_{-0.08}$
00034673096	2017-03-23	229	PC	15	15/30	undetected
00034673097	2017-03-24	104	PC	15	15/30	undetected
00034673098	2017-03-26	192	PC	15	15/30	undetected

Note. — §: Spectra are unavailable due to short exposure times and low flux.

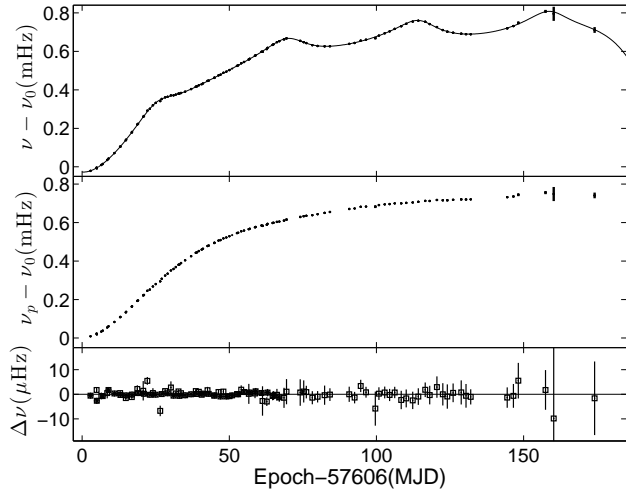


Figure 3. The spin frequencies without the orbital correction are plotted versus time (begin time: MJD 57606) in the upper panel ($\nu_0 = 0.128\text{Hz}$), while the frequencies shown in the middle panel have been orbitally corrected. The bottom panel shows fitting residuals of the spin and orbital parameters. The filled square data are adopted from the *Fermi*/GBM results.

frequencies are searched without considering the spin evolution; (2) Fit the spin parameters and orbital elements; (3) Search spin frequencies considering the spin evolution and orbital modulation; (4) Repeat steps (2) and (3) for several times to get the best spin parameters and orbital elements. The fitting in step (2) is based on the Levenberg-Marquardt algorithm for non-linear least square method, weighted by the error of each point, which is similar to the fitting process described in Li et al. (2011, and references therein). The spin frequency errors of GBM are multiplied by a factor of 5 to balance the weights between XRT and GBM in the fitting process. The best fitted parameters listed in Table 2 are quite consistent with those reported in Townsend et al. (2017) and the uncertainties of parameters is 1σ .

It is difficult to obtain the derivative of the spin frequency with each individual observation alone. Alternatively, we calculate the spin-up rates from the fitting results and the X-ray fluxes for each two successive observations, and plot them in Figure 5.

4. DISCUSSION & CONCLUSIONS

During the 2016-2017 giant outburst, the X-ray luminosity of SMC X-3 reached a peak value $\sim 10^{39}$ erg/s (in 0.6–10 keV) around August 24, that is a few times of NS Eddington luminosity and close to the low-luminosity tail of ULXs. Since 2017 January, the source flux dropped sharply with two humps separated by about one orbital period (~ 42 d), and becomes lower than the detection limit of *Swift*/XRT (Figure 1). Its X-ray spectra become harder as flux decays. The BAT daily light curve shows an indication of flat plateau during MJD $\sim 57618 - 57640$. The magnitudes in the near-ultraviolet bands increased by $\sim 0.2^m - 0.3^m$ during outburst, and returned to a constant level after two months. Alternatively, the U band flux changes with the XRT count rates with the Spearman’s rank correlation coefficients of $\rho/P = 0.86/3.6 \times 10^{-10}$.

According to the *Doppler* motion of the binary, we fit the orbital modulation of the observed pulse period, ob-

Table 2
Timing results of SMC X-3 from the X-ray Observations

Parameters	Value
R.A.	$00^h 52^m 05^s .64$
Decl.	$-72^\circ 26' 04''.2$
Epoch(MJD)	57606
ν (mHz)	128.005(2)
$\dot{\nu}$ (10^{-5}Hz d^{-1})	-0.10(5)
$\ddot{\nu}$ (10^{-6}Hz d^{-2})	2.08(7)
ν_3 (10^{-7}Hz d^{-3})	-1.88(7)
ν_4 (10^{-8}Hz d^{-4})	1.1(4)
ν_5 (10^{-10}Hz d^{-5})	-3.9(2)
ν_6 (10^{-12}Hz d^{-6})	8.9(5)
ν_7 (10^{-13}Hz d^{-7})	-0.96(7)
Porb(d)	44.52(9)
asini(light-second)	194(1)
e	0.259(3)
ω°	202(2)
T_ω (MJD)	57632.1(3)
$\chi^2_{r,e}$ (MJD)	1.1
d.o.f.	89

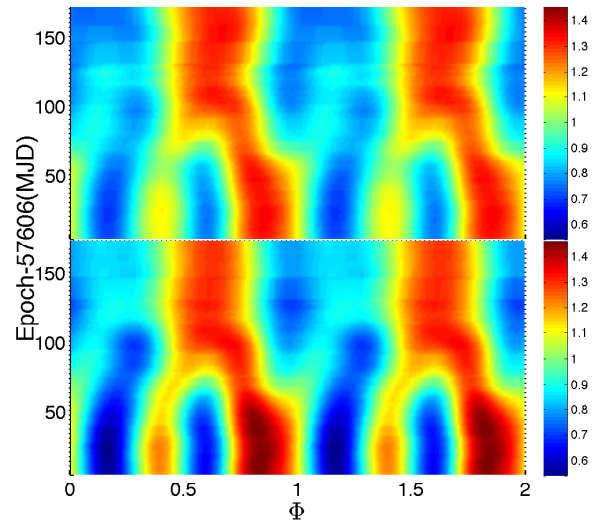


Figure 4. Evolution of the background-subtracted pulse profiles in 0.5-2 keV (upper panel) and 2-10 keV bands (bottom panel). The color bar marks the normalized CR.

tain an orbital period of $P = 44.52 \pm 0.09$ days that is consistent with the previous works to within 3σ uncertainty (Galache et al. 2008; Bird et al. 2012), and determine the projected semi-major axis $asini = 194 \pm 1$ light seconds and an eccentricity of $e = 0.259 \pm 0.003$. After correcting for the orbital motion, we find that the spin frequency increases steadily, indicating the formation of a transient accretion disk surrounding the central NS during the outburst. According to the accretion torque theory, we would expect the spin-up rate increases with the accretion rate ($\dot{\nu} \propto \dot{M}^{6/7}$) (Ghosh & Lamb 1979; Wang 1981). The power-law relationships between $\dot{\nu}$ and X-ray luminosity have been confirmed in some BeXBs during their type II giant outbursts and consistent with the results of QPOs evolution (e.g. Finger et al. 1996; İcđem et al. 2011; Sartore et al. 2015). However, the fitted power-law indices are generally greater than the prediction of 6/7. Alternatively, fitting the spin-up rate and

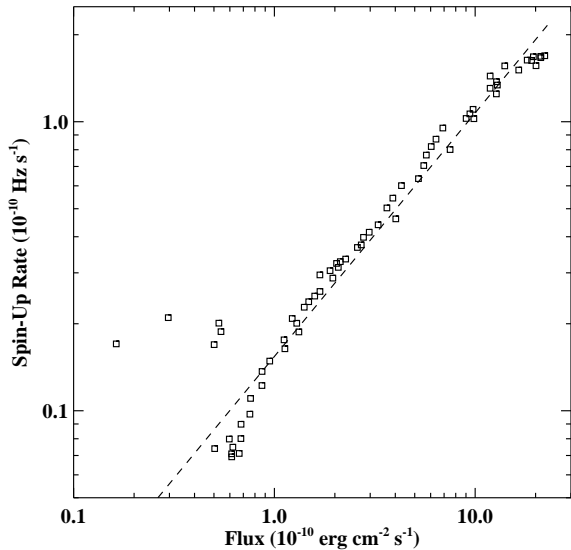


Figure 5. Relationship between the 0.6-10 keV unabsorbed flux and the spin-up rate during the 2016 super-Eddington outburst. The dashed line is the best-fit power-law with an index of 0.84 ± 0.02 . Note that, the spin-up rates for the five data points well above the dashed line have large uncertainties and are consistent with zero within 2σ .

the 0.6–10 keV flux of SMC X-3 with a power-law, we obtain an index of 0.84 ± 0.02 that is in agreement with $6/7$, but the relation deviates from the power-law at the peak and the low luminosity (Figure 5).

Klus et al. (2014) investigated all *RXTE*/PCA data to determine the long-term average spin period ($P = 7.7836 \pm 0.0001$ s), spin-down rate ($\dot{P} = 0.00262 \pm 0.00003$ s yr $^{-1}$), and the average X-ray luminosity ($L_X \sim 3.7 \times 10^{36}$ erg/s) for SMC X-3. These results point to a torque switch from spin-down to spin-up at the beginning of the giant outburst ($L_X < 10^{38}$ erg/s). By assuming spin equilibrium, they derived a magnetic field of $\sim 2.9 \times 10^{12}$ G. Here, we report the instantaneous spin period measurements during the 2016 giant outburst. The spin frequency with the orbital correction is evidently near the torque equilibrium with the spin frequency derivative close to zero at an unabsorbed luminosity of $\sim L_X \sim 2 \times 10^{37}$ erg/s assuming the distance of 62.1 kpc (Figs 3 and 5). Thus, we can estimate a magnetic field of SMC X-3 with the assumption of $R_{co} = R_m$, or $B = [4.8 \times 10^{10} P^{7/6} (\frac{flux}{10^{-9} \text{ erg cm}^{-2} \text{ s}^{-1}})^{1/2} \times (\frac{d}{1 \text{ kpc}}) \times (\frac{M}{1.4 M_\odot})^{1/3} \times (\frac{R}{10^6 \text{ cm}})^{-5/2}]$ G for the simplified model (Cui 1997), yielding $B \sim 6.8 \times 10^{12}$ G with the canonical value of NS mass and radius, i.e. $1.4 M_\odot$ and 10 km. That is, the obtained value is significantly higher than that reported by Klus et al. (2014).

Interestingly, if taking the color correction factor into account, the emission size of the thermal component ($R_{BB} \sim 1000$ km) detected during the source returning to the quiescence state is significantly larger than the NS radius. Alternatively, the spin periodic modulation indicates that the BB emission is not homogenous, but comes from the place even farther away from the central NS. The location where the thermal component is

produced could be close to the corotation radius of SMC X-3 ($R_{co} \sim 6000$ km), supporting the torque equilibrium hypothesis. The emission line detected in XMM-Newton data is consistent with that from the highly ionized Fe XXV, which could originate from the illumination of cold material (i.e. the cool BB component) by central hard X-rays. The relatively large line widths ($\sigma = 0.35_{-0.10}^{+0.14}$ keV) can be interpreted as the results of Keplerian rotation at a radius of ~ 1000 km, which agrees with the size of the BB component discussed above. We, however, caution that the broad emission line with the central energy of 6.65 keV could be due to the blending of lines from different ionisation states of Fe, i.e. Fe K α and Fe K β , which have been detected in other accreting pulsars (e.g. Reynolds & Miller 2010).

After 2017 January, the flux drops abruptly, which gives the hint of “propeller” effect as the result of the further decrease in accretion rate and that the centrifugal force prevents material from entering the magnetosphere. It is worth to note that there are two X-ray flux jumps exhibited around MJD 57780 and 57822 (corresponding to the orbital phase of ~ 0.3) in Figure 1, and they can be interpreted as the increase in mass accretion rate when the NS travels through its periastron, i.e. Type I outbursts. Since the typical X-ray luminosity of its Type I outburst is above the *Swift*/XRT detection limit, we expect that the periodic outbursts can be observed by the future *Swift* monitoring data. However, these outbursts are beyond the scope of this paper, and we suggest that the source has ended its 2016-2017 giant outburst in the end of 2017 March.

At low luminosity, the single peak pulse profiles were observed in the *RXTE* (Galache et al. 2008), *Chandra* and *XMM-Newton* archival data (Haberl et al. 2008) more than ten years ago. As shown explicitly in Figure 4, the pulse profiles of SMC X-3 during the 2016 outburst are variable and have double peaks at the beginning of the outburst, and then converges to a single peak as the flux decays below $L_X \sim 4 \times 10^{37}$ erg/s. The similar evolution pattern of pulse profiles has been reported in other outbursts but with lower transient luminosity, e.g. the 1994 giant outburst of A0535+262 (Bildsten et al. 1997). These results can be interpreted as different geometries of the accretion column at beyond and below the critical luminosity ($\sim 10^{37}$ erg/s; e.g. Basko & Sunyaev 1976; Becker et al. 2012; Mushtukov et al. 2015a; Sartore et al. 2015), respectively. At lower luminosity, the in-falling gas may be decelerated via Coulomb interactions and a pencil-beam of emission is formed. At the supercritical state, the accretion flow is decelerated via the radiative shock and the photons can only escape from accretion column walls resulting in double peaks structure (i.e. fan beam mode; e.g. Becker et al. 2012). As can be seen in Figure 1, the pulse fraction generally increases with the hardness during the outburst, which is consistent with those recently found in ULXs. Investigating a sample of ULX broadband X-ray spectra, Pintore et al. (2017) suggested that the ULX pulsars have harder spectra than that of the majority of other ULXs and the spectra became softer when no pulsations are detected. It is worth to note that the luminosity of all three accreting NSs can be two orders of magnitude higher than that of SMC X-3 but

all have single peak pulse profiles (Bachetti et al. 2014; Fürst et al. 2016; Israel et al. 2016, 2017). More extreme surface magnetic fields are required to account for the observed characteristics of ULX pulsars.

We thank the anonymous referee for his/her helpful comments. S.S.W. thanks Dr. Kim Page from *Swift* team for discussions on data analysis. We thank Jian Li, Xiao-Chuan Jiang and Fang-Jun Lu for many valuable suggestions. This work is supported by the National Natural Science Foundation of China under grants 11303022, 11133002, 11233001, 11573023, 11173016, 11673013, 11373024, 11233003, 11503027, 11622326 and 11433005, National Program on Key Research and Development Project (Grant No. 2016YFA0400802 and 2016YFA0400803), and by the Special Research Fund for the Doctoral Program of Higher Education (grant No. 20133207110006).

REFERENCES

- Bachetti, M., Harrison, F. A., Walton, D. J., et al. 2014, *Nature*, 514, 202
- Basko, M. M., & Sunyaev, R. A. 1976, *MNRAS*, 175, 395
- Becker, P. A., Klochkov, D., Schönherr, G., et al. 2012, *A&A*, 544, A123
- Bildsten, L., Chakrabarty, D., Chiu, J., et al. 1997, *ApJS*, 113, 367
- Bird A. J., Coe M. J., McBride V. A., & Udalski A., 2012, *MNRAS*, 423, 3663
- Cash, W., 1979, *ApJ*, 228, 939
- Campana, S., Brivio, F., Degenaar, N., et al. 2014, *MNRAS*, 441, 1984
- Chen, W.-C., 2017, *MNRAS*, 465, L6
- Christodoulou, D. M., Laycock, S. G. T., Yang, J., & Fingerman, S. 2016, *ApJ*, 829, 30
- Clark, G., Doxsey, R., Li F., Jernigan, J. G., & van Paradijs, J. 1978, *ApJ*, 221, L37
- Coburn, W., Heindl, W. A., Rothschild, R. E., et al. 2002, *ApJ*, 580, 394
- Corbet, R. H. D., Edge, W. R. T., Laycock, S., Coe, M. J., Markwardt, C. B., & Marshall, F. E. 2003, *AAS High Energy Astrophys.*, 7, 17.30
- Cowley, A. P., & Schmidtke, P. C. 2004, *AJ*, 128, 709
- Cui, W. 1997, *ApJ*, 482, L163
- Cutri, R. M., Skrutskie, M. F., van Dyk, S., et al. 2003, *yCat*, 2246, 0
- Dickey, J. M., & Lockman, F. J. 1990, *ARA&A*, 28, 215
- Edge, W. R. T., Coe, M. J., Corbet, R. H. D., Markwardt, C. B., & Laycock, S. 2004, *Astron. Telegram*, 225, 1
- Eksi, K. Y., Andaç, İ. C., Çikintoğlu, S., et al. 2015, *MNRAS*, 448, L40
- Finger, M. H., Wilson, R. B., & Harmon, B. A. 1996, *ApJ*, 459, 288
- Fürst, F., Pottschmidt, K., Wilms, J., et al. 2014, *ApJ*, 780, 133
- Fürst, F., Walton D.J., Harrison F.A., et al., 2016, *ApJL*, 831, L14
- Galache, J.L., Corbet, R.H.D., Coe, M.J., et al. 2008, *ApJS*, 177, 189
- Gehrels, N., Chincarini, G., Giommi, P., et al. 2004, *ApJ*, 611, 1005
- Ghosh, P., & Lamb, F. K. 1979, *ApJ*, 234, 296
- Goodman, J., & Weare, J., 2010, *camcos*, 5, 1
- Graczyk, D., Pietrzyński, G., Thompson, I. B., et al. 2014, *ApJ*, 780, 59
- Grimm, H. J., Gilfanov, M., & Sunyaev, R. 2002, *A&A*, 391, 923
- Haberl F., Eger P., Pietsch W., 2008, *A&A*, 489, 327
- Hilditch, R. W., Howarth, I. D., & Harries, T. J. 2005, *MNRAS*, 357, 304
- Hogg, D. W., Bovy, J., & Lang, D. 2010, arXiv:1008.4686
- İçdem, B., İnam, S., & Baykal, A. 2011, *MNRAS*, 415, 1523
- Israel, G.L., Belfiore, A., Stella, L., et al., 2016, arXiv:1609.07375
- Israel G.L., Papitto A., Esposito P., et al., 2017, *MNRAS*, 466, L48
- Kawashima, T., Mineshige, S., Ohsuga, K., & Ogawa, T. 2016, *PASJ*, 68, 83
- Kennea, J. A., Coe, M. J., Evans, P. A., et al., 2016, *Astron. Telegram*, 9362, 1
- King, A., & Lasota, J.-P., 2016, *MNRAS*, 458, L10
- Klus, H., Ho, W. C. G., Coe, M. J., Corbet, R. H. D., & Townsend L. J., 2014, *MNRAS*, 437, 3863
- Krimm, H. A., Holland, S. T., Corbet, R. H. D., et al. 2013, *ApJS*, 209, 14
- Li, J., Wang, W., & Zhao, Y. H. 2011, *MNRAS*, 423, 2854
- Lamb, F. K., Pethick, C. J., & Pines, D. 1973, *ApJ*, 184, 271
- McBride, V.A., M.J. Coe, I. Negueruela, I., Schurch, M. P. E. & McGowan, K. E., 2008, *MNRAS*, 388, 1198
- Mineo, S., Gilfanov, M., & Sunyaev, R. 2012, *MNRAS*, 419, 2095
- Mushtukov, A. A., Suleimanov, V. F., Tsygankov, S. S., & Ingram, A. 2017, *MNRAS*, tmp, 143
- Mushtukov, A. A., Suleimanov, V. F., Tsygankov, S. S., & Poutanen, J. 2015, *MNRAS*, 447, 1847
- Mushtukov, A. A., Suleimanov, V. F., Tsygankov, S. S., & Poutanen, J. 2015, *MNRAS*, 454, 2539
- Negoro, H., et al., 2016, *Astron. Telegram*, 9348, 1
- Pan, Y.Y., Song, L. M., Zhang, C. M., & Tong, H. 2016, *MNRAS*, 461, 2
- Pintore, F., Zampieri, L., Stella, L., Wolter, A., Mereghetti, S., Israel, G. L., 2017, *ApJ*, 836, 113
- Pottschmidt, K., Ballhausen, R., Wilms, J., et al. 2016, *Astron. Telegram*, 9404, 1
- Reig, P., 2011, *Ap&SS*, 332, 1
- Reynolds, M. T., & Miller, J. M. 2010, *ApJ*, 723, 1799
- Sartore, N., Jourdain, E., & Roques, J.-P. 2015, *ApJ*, 806, 193
- Scowcroft, V., Freedman, W. L., Madore, B. F., et al. 2016, *ApJ*, 816, 49
- Shao, Y., & Li, X.-D., 2015, *ApJ*, 802, 131
- Shi, C.-S., Zhang, S.-N., & Li, X.-D. 2015, *ApJ*, 813, 91
- Sturm, R., Haberl, F., Pietsch, W., et al. 2013, *A&A*, 558, A3
- Townsend, L. J., Kennea, J. A., Coe, M. J., et al., 2017, arXiv:1701.02336
- Tsygankov, S. S., Doroshenko, V., Lutovinov, A. A., Mushtukov, A. A., & Poutanen, J. 2017, *A&A* submitted, arXiv:1702.00966
- Tsygankov, S. S., Mushtukov, A. A., Suleimanov, V. F., & Poutanen, J. 2016, *MNRAS*, 457, 1101
- Walter, R., Lutovinov, A. A., Bozzo, E., & Tsygankov, S. S. 2015, *A&A Rev.*, 23, 2
- Wang, Y.-M. 1981, *A&A*, 102, 36
- Weng, S.-S., Ge, M.-Y., Zhao, H.-H., Wang, W., & Zhang, S.-N. 2016, *Astron. Telegram*, 9731, 1
- Weng, S.-S., & Zhang, S.-N. 2011, *ApJ*, 739, 42
- Yan, J.-Z., Chaty, S., Zurita Heras, J. A., Li, H., & Liu, Q.-Z., 2012, *ApJ*, 753, 73
- Yang, J., Laycock, S. G. T., Christodoulou, D. M., et al. 2017, *ApJ*, 839, 119
- Zaritsky, D., Harris, J., Thompson, I. B., Grebel, E. K., & Massey, P. 2002, *AJ*, 123, 855